International Journal of Recent Technology and Engineering (IJRTE)
ISSN: 2277-3878, Volume-8 Issue-5, January 2020

Improved Erosion Resistance by HVOF Sprayed 10%Al_2O_3-COCrAlTaY Coating on Ti-31

Anand Babu K, N. Jegadeeswaran, Kapilan N, Ramesh M R

Abstract*: *In this present research work the solid particle erosion test carried on uncoated samples (Ti-31), and HVOF sprayed 10%Al_2O_3-CoCrAlTaY on Ti-31 are made. Erosion test are done with impact angles of 30º, 60º and 90º. Solid particle erosion studies were carried out using air jet erosion test rig as per ASTM G76-02 standard.All the three angles of uncoated alloys exhibit erosion damage under ductile mode and less amount of erosive loss compared HVOF coated samples. The HVOF sprayed coated Ti-31 at various impact angles is brittle mode. The mechanism of material removal during erosion of brittle materials is explained by using SEM micrographs.

Keywords* : *Solid particle erosion, HVOF coatings, SEM.

I. INTRODUCTION

Titanium alloys have been increasingly used in aerospace, biomedical, and chemical industries due to their very high strength to weight ratio, good fatigue, biocompatibility and high corrosion resistance. Although titanium based alloys exhibit good corrosion resistance due to the formation of titania on its surface, the nature, composition and thickness of the protective oxide scales depend on environmental conditions [1]. Erosion is a major cause of degradation of turbine components.

Erosive wear is caused in the solid bodies by the action of sliding or impact of solids, liquids, gases or a combination of these [2]. Erosion can be divided in to three basic types: Solid particle erosion, liquid impact erosion and cavitation erosion. Cavitation erosion is the loss of material due to the repeated formation and collapse of bubbles in a liquid. Liquid impact erosion is the damage by water droplets. Solid particle erosion involves the impact of solid particles on a solid surface. Solid particle erosion is an important material degradation mechanism encountered in a number of engineering systems such as thermal power plants, aircraft gas turbine engines, pneumatic bulk transport systems, coal liquefaction/gasification plants and ore or coal slurry pipe lines. At the same time, the erosion process has been used as beneficial one in a number of situations like sand blasting of castings, shot peening of rotating components, cutting of hard and brittle materials by abrasive jets and rock drilling [3].

Manuscript received on January 02, 2020.
Revised Manuscript received on January 15, 2020.
Manuscript published on January 30, 2020.

***** Correspondence Author
Anand Babu K*, School of Mechanical Engineering, REVA University, Bengaluru India. Email: anbamech@gmail.com
Dr. N. Jegadeeswaran, School of Mechanical Engineering, REVA University, Bengaluru India. Email: njagadeeswaran@reva.edu.in
Dr. Kapilan N, Department of Mechanical Engineering, Nagarjuna College of Engineering and Technology, Bengaluru India. Email:kapil_krecmech@yahoo.com
Dr. Ramesh M R, Department of Mechanical Engineering, National institute of Technology , Surathkal,India. Email: rameshmr@nitk.edu.in

II. EXPERIMENTAL DETAILS

A. Substrate Material and Coating Formulation

Substrate material of Titanium alloy (Ti-31), Which is used as a candidate material for turbine blades were procured from Mishra Dhatu Nigam Limited, Hyderabad, India. The stated composition of the substrate material is given in the Table I. Material was brought in sheet form and coupons of size 25 mm X 25 mm X 5 mm were cut and used for deposition. Substrate steels were grit-blasted with Al_2O_3 before HVOF spraying to develop better adhesion between the substrate and the coating.

Table I Chemical compositions of the substrate used for HVOF coating.

Sl. No	Substrate	Chemical composition	ASTM Grade
1	Titanium Alloy (Ti-31)	Ti-6Al-4V	ASTM B338 Grade 5

Coating Powder was chosen based on their resistance against hot corrosion and erosion. The Oxide alloy powder of 10%Al2O3+90% (Bal Co-23Cr-7Al-9Ta-0.68Y) was used as the feedstock alloy for HVOF spraying. The details of the feedstock alloy used and HVOF coating are given in Table II. HVOF spraying was carried out using METCO DJ2600 equipment, which utilizes a supersonic jet generated by the combustion of liquid petroleum gas and oxygen mixture. The HVOF coating process was carried out in Spray met Coating Industries, Bangalore, India and Anod Plasma Industries, Kanpur, India. The spraying parameters employed during HVOF deposition were listed in Table 3 and kept constant throughout coating process.

B. Erosion Studies

Room temperature, solid particle erosion studies were carried out using air jet erosion test rig as per ASTM G76-02 standard(Figure 1). Tests were conducted at the Surface Engineering Laboratory, PESIT, Bangalore, India. The erosion studies were performed on uncoated as well as coated samples for the purpose of comparison.

The samples was first cleaned in acetone using an ultrasonic cleaner, dried and then weighed using an electronic balance with least count of 0.01 mg.

The samples was then fixed to the sample holder of the erosion test rig and eroded with silica sand at the predetermined particle feed rate, impact velocity and impact angle for period of about 5 min. The samples was then removed, cleaned in actone and dried and weighed to determine the weight loss (i.e., testing time x particle feed rate) was then computed as the dimensionless incremental erosion rate. The above procedure was repeated till the incremental erosion. Erodent material is silica sand and size is 125-180(µm).The particle velocity is 40(m/s) and feed rate is 5(g/min).

Table II Composition of the feedstock alloy

Sl. No.	Coating powder	Chemical composition	Shape	Particle size
1	Oxide alloy powder	10%Al2O3+90%(Bal Co-23Cr-7Al-9Ta-0.68Y) (Fused powder) Powder Alloy Corporation, Cincinnati, Ohio	Spher -ical	-45 to +15µm

III. RESULTS AND DISCUSSION

A. Uncoated Ti-31 Alloy

The photographs of the erosion scar produced on the Ti-31 sample, with 30º, 60º and 90º of erodent impact angle are shown in Fig. 1 a, b, c, respectively. The centre portion of the eroded scar (A) represents localized region of material removal and it is surrounded by a region of elastically loaded material (B). The loss in weight of the sample after each 5 minutes is measured and using weight loss and mass of the erodent, erosion rate is measured as follows:

Erosion rate (g/g) = Cumulative weight loss of sample/ Mass of erodent. An erosion rate curve is drawn as a plot of erosion rate versus cumulative mass of the erodent, for each erodent impact angle.

Steady state volume erosion rate is estimated as follows:

Steady state volume erosion rate (cm^3/g) = Average of erosion rate/ Density.

The erosion rate curves along with the bar chart indicating the steady state volume erosion rate are shown in Fig. 2. From Figure 2a, the sample shows highest erosion rate, when it is impacted at 30º and minimum erosion rate when it is impacted at 90º. Similar trend is observed in steady state volume erosion rate (Fig. 2b) also. This is characteristic behaviour of materials which exhibit ductile mode of erosion [2].

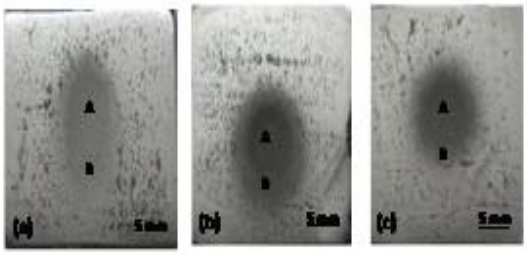

Fig. 1 Macrographs of uncoated Ti-31 alloy impacted by silica erodent at different angles (a) Impact angle of 30º (b) Impact angle of 60º c) Impact angle of 90º.

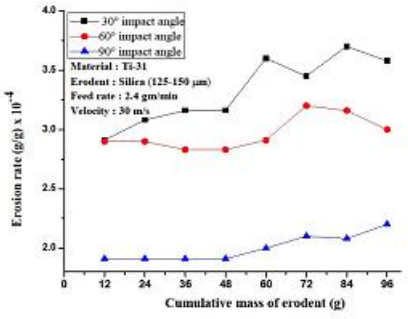

(a)

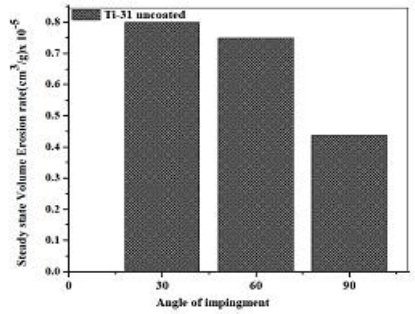

(b)

Fig. 2 Plot of erosion rate versus cumulative mass of erodent of uncoated Ti-31 alloy subjected to erosion at 30º, 60º and 90º impact angle (a) Variation of the erosion rate (b) Histogram illustrating the steady state volume erosion rate.

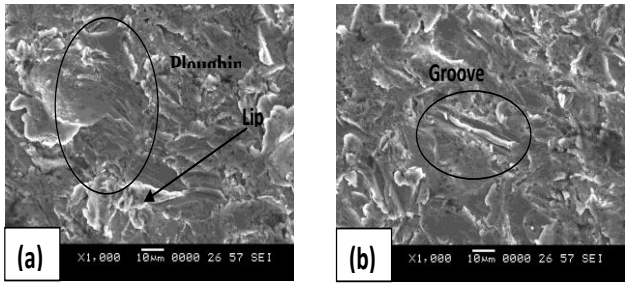

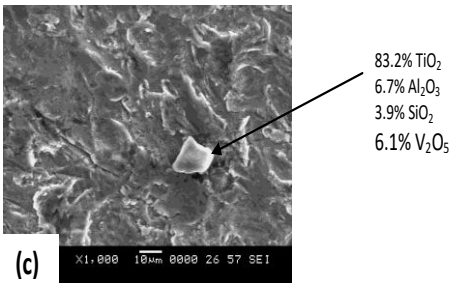

Fig. 3 SEM micrographs showing the morphology of eroded Ti-31 at an impact angle of 30º.

Figure 3 shows the micrographs of erosion scar produced on uncoated Ti-31, at an impact angle of 30º. The micrographs show clear indications of material damage in the form ploughing (Fig. 3a), groove (Fig. 3b) and loose debris (Fig. 3c).

The loose debris is predominantly Ti. Ploughing of the sample surface by the erodent particles is a common method of material removal and SEM micrographs indicate it.

Ploughing takes place extensively at 30º impact angle compared to 90º (Fig. 4)impact angle, for all three uncoated samples. SEM micrographs also indicate severe plastic deformation along with ploughing. The hard silica particles have sheared the material towards sides and in turn produced material lips. Erosion damage with plastic deformation is common in the case of ductile materials. It is reported that ductile materials show more erosion wear at lower impact angles and ploughing is an important mode of wear damage. At impact angles of 60º (Fig. 4)and 90º(Fig. 4), erosive loss is less compared to 30º impact angle. This is due to embedment of silica particles (erodent) in the target material and this is more at higher impact angle. This acts as a shield against further impacting particles.In few situations, the embedded silica particles have fallen off and this has resulted in the formation of cavities. The cavities increase the rate of erosion loss.

Figure 4 shows the micrographs of erosion scar on uncoated Ti-31. Fig. 4a(60^0) shows material damage in the form of ploughing. In Fig.4b(60^0), the entrapment of the erodent (SiO2) within the substrate Ti-31 is observed and in Fig.4c(60^0), the crater created when the embedded erodent is fallen off during the erosion process is presented. In Figure 4, microstructures on the scar produced due to normal impact (90º) of erodent on the uncoated Ti-31 are presented. Microstructures present evidences for ploughing (Fig 4a-90º), embedment of silica erodent (Fig 4b-90º) and groove (Fig 4c-90º)

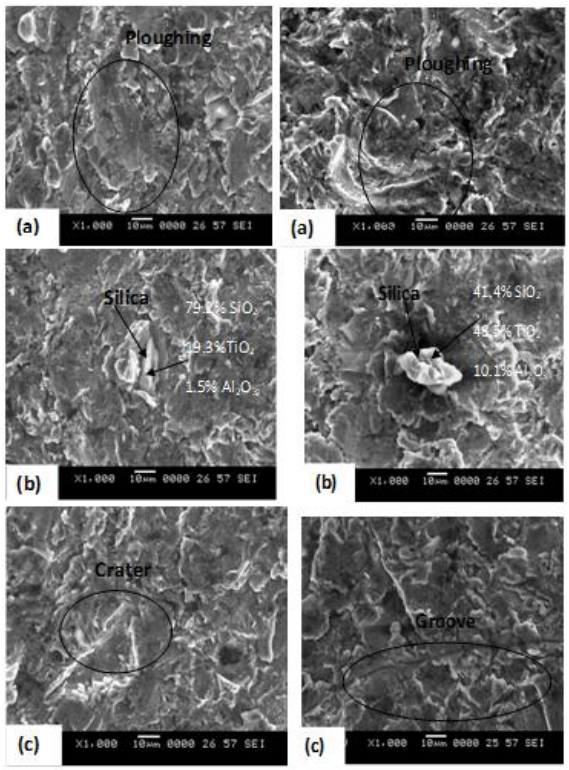

Fig. 4 SEM micrographs showing the morphology of eroded surfaces on uncoated Ti-31, with an impact Angles of 60º and 90^0.

B. Solid Particle Erosion Studies On Coated Samples

Solid particle erosion studies were done on 10% Al_2O_3 + CoCrAlTaY, coated Ti-31 sample. Al-Fadhli et al. [17] reported that the erosion resistance of HVOF sprayed coating is independent type of substrate. In this investigation, only Ti-31 is used as substrate for investigation of erosion behaviour.

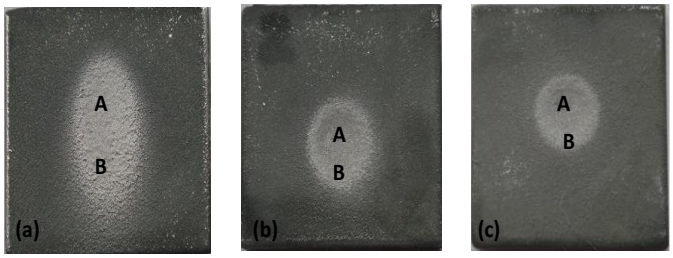

Fig. 5 Macrographs of 10% Al_2O_3-CoCrAlTaY coated Ti-31 impacted by silica erodent at different angles (a) Impact angle 30º (b) Impact angle 60º (c) Impact angle 90º.

Fig. 5 shows the macrographs of the erosion scar produced on the 10% Al_2O_3-CoCrAlTaY coated Ti-31, using silica as erodent. The erosion scar produced using impact angles of 30º, 60º and 90º is shown in Fig. 5a, 5b and 5c respectively. The plots of erosion rate as a function of cumulative mass of erodent and steady state volume erosion rate as a function of impact angle are presented in Fig. 6a and 6b, respectively. The plot shows that (Fig. 6a), after the initial transient, the erosion rate becomes stabilised to a constant value and the stabilised value is highest for the impact angle of 90º and the lowest for the impact angle of 30º. This is also presented in the plot of steady state volume erosion rate versus impact angle (Fig. 6b). The bar chart shown in Fig. 6b is similar to the damage of brittle materials under erosion conditions [18, 19]. Generally, brittle materials exhibit more erosive loss at impact angle of 90º compared to that at 30º.

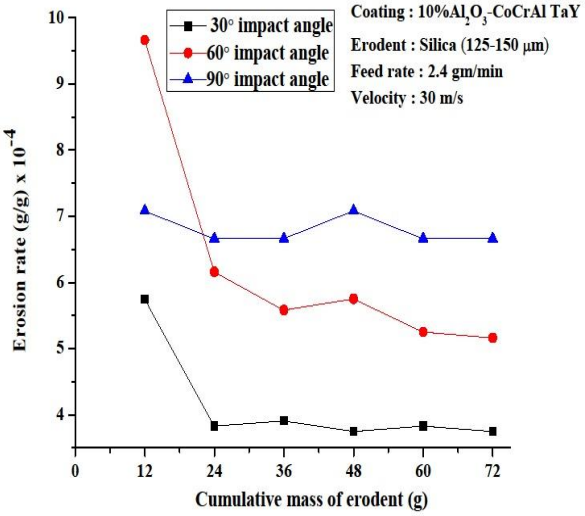

(a)

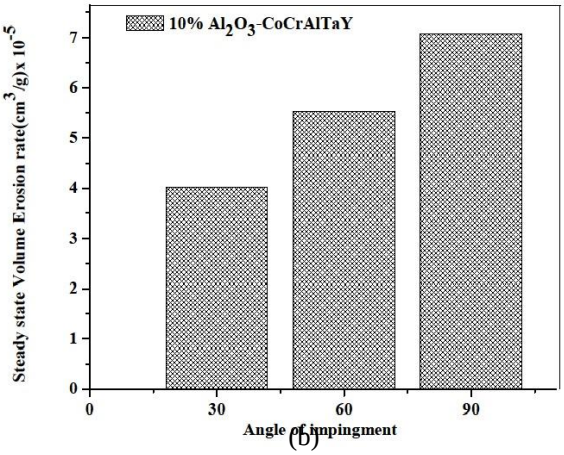

Fig. 6 Plot of erosion rate versus cumulative mass of erodent of 10%Al_2O_3-CoCrAlTaY coated Ti-31 subjected to erosion at 30º, 60º and 90º impact angle (a) Variation of the erosion

rate (b) Histogram illustrating the steady state volume erosion rate.

Figure 7 shows micrographs of the eroded scar produced in 10% Al_2O_3-CoCrAlTaY coated Ti-31, using an impact angle of 30º. Micrographs clearly indicate the material damage by crater formation (Fig. 7a), crack formation (Fig. 7b) and attachment of silica erodent (Fig. 7c). Though the silica particle is sticking to the coated surface, they are not embedded as observed in the case of uncoated samples. Figure 8 shows typical microstructures observed in the scar produced with an impact angle of 60º. Following features are observed in the micrographs. Fig. 8a shows formation of cracks and lips during the impact with silica particles; Fig. 8b shows the attachment of silica particle, Fig. 8c shows the Al_2O_3 pull out particles during erosion and Fig. 8d shows the crater created due to removal of particle from the surface.

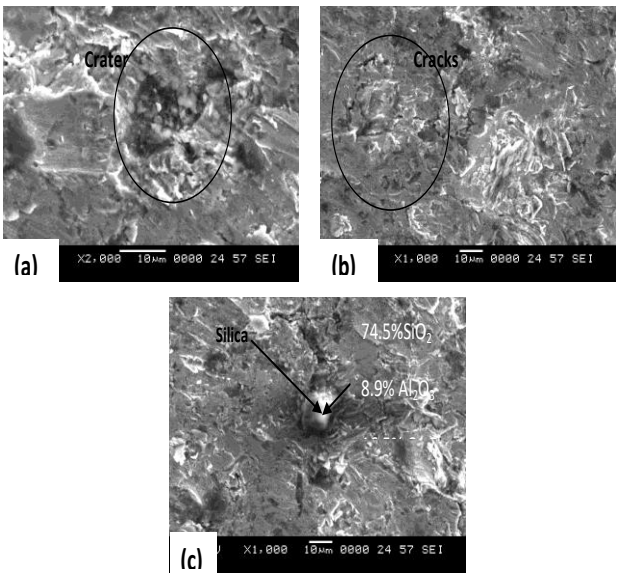

Fig. 7 SEM micrographs showing the morphology of eroded surface on 10% Al_2O_3-CoCrAlTaY coated Ti-31, with an impact angle of 30º.

The micrographs of the scar produced during the erosion with an impact angle of 90º are presented in Fig. 9. Fig. 9a and shows the crater and Fig. 9b shows the micrograph with indications of crack, Fig. 9c shows groove formation due to cutting action of hard silica particles and Fig. 9d shows the attachment of erodent particles on the coated surface.

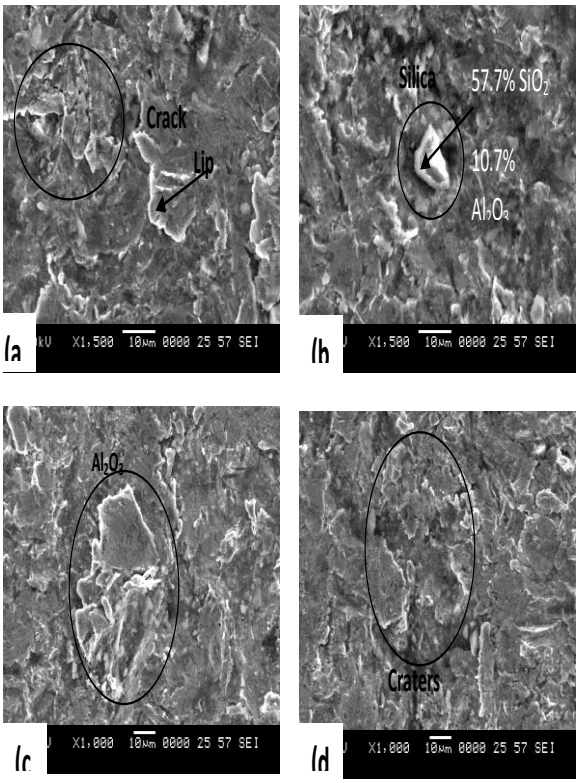

Fig. 8 SEM micrographs showing the morphology of eroded surface on 10% Al_2O_3-CoCrAlTaY coated Ti-31, with an impact angle of 60º.

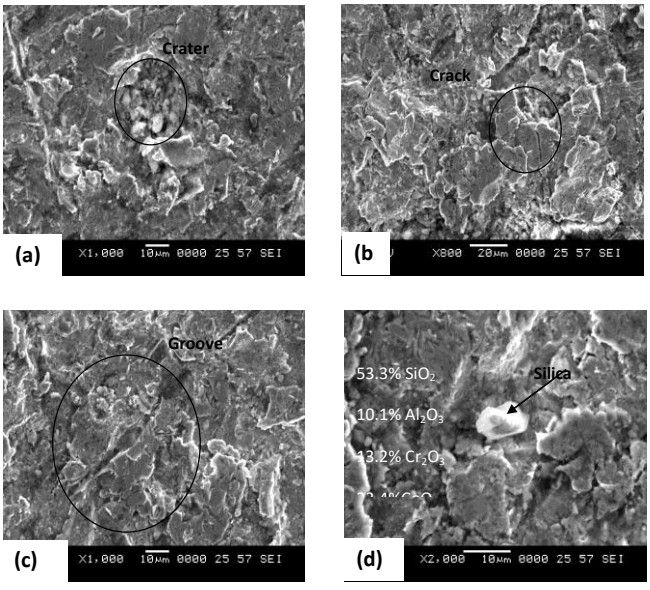

Fig. 9 SEM micrographs showing the morphology of eroded surface on 10% Al_2O_3-CoCrAlTaY coated Ti-31, with an impact angle of 90º.

Retrieval Number: D8864118419/2020©BEIESP
DOI:10.35940/ijrte.D8864.018520
Journal Website: www.ijrte.org

Published By:
Blue Eyes Intelligence Engineering
& Sciences Publication

IV. DISCUSSION

Fig. 7 shows variation of erosion rate as a function of cumulative mass of erodent for the HVOF sprayed 10%Al_2O_3-CoCrAlTaY coated Ti-31 at various impact angles. The material loss is higher at 90º impact angle compared to 30º and 60º impact angles. Dramatic increase in the erosion rate at higher impact angle (near to 90º) compared to impact angles of 30º or 60º indicates that the material behavior is brittle under solid particle erosion conditions [3]. Initially high erosion rates are observed (Fig. 6a) as a result of rough outer surface of the as-sprayed coatings (Ra of as sprayed coating-4.1µm,). The globular protuberances on the as-sprayed surface are smoothened out by the impacting particles and the lower steady state erosion condition is reached with the increased cumulative mass of the erodent.

The mechanism of material removal during erosion of brittle materials is explained by Sheldon and Finnie, (1966) [20]. It is generally thought that when erodent is sub millimeter scale and angular in shape, erosion occurs by lateral (or conical) cracking. During repeated impacts of hard, erosive particles lateral cracks are formed. Subsequently, they intersect and loosen the chunk of the material which will be removed during next impact, [21]. It is also thought that the similar damage mechanism is active under both normal and oblique impact conditions [13].

The coating microstructure can be considered as a composite microstructure consisting of a hard phase (consisting of alumina) embedded in a relatively soft matrix made of metallic constituents. In such systems, Soderberg [22] suggested that the relative value of erodent particle size with respect to microstructural scale affects damage mechanism. When erodent particle size is larger compared to microstructural length scale, the damage due to individual impact overlaps the microstructural features and the damage within the feature is constrained by other features. In such cases the damage is mainly due to hard phase cracking and its dislodgement leading to formation of craters at the surface. The crater formation is also possible if hard, angular particle impacts the soft matrix at an angle and in turn dislodges the particle from its site. Soderberg [22] believes that for this to happen, interfacial strength between soft phase and hard phase must be small.

The SEM micrographs showing the details of microstructural features in scars produced with impact angles of 30º, 60º and 90º shows a multiple modes of damage activity. The cracks are observed in all three impact angles (Fig. 7, Fig. 8 and Fig. 9). Most of the cracks are multiple in nature and limited to local regions. Extending the logic presented by Soderberg et al. [22], we conclude that cracks are generated in Al_2O_3 phase. The propagation of the crack is limited by the presence of soft phase surrounding the hard phase. This limits the damage by the erodent particles.

The SEM micrographs shown in Fig. 7, Fig. 8 and Fig. 9 also indicate that the crater formation is extensive. Coarse, partially molten splats have disintegrated during impact with hard erodent particles and the cracks which are generated during disintegration got connected and separated from the bulk of the coating. Also, in the process they have created small craters. In few locations, complete hard phase have come out. This happens at those locations, where interface is poor due to partial melting of the powders during HVOF spraying. Also, some amount of local oxidation will take place during the flight of semi molten splat from the HVOF gun towards the sample surface. The oxidation will reduce the bond between depositing splats. Fig. 8d shows a crater formed predominantly in the softer binder region, leading to dislodging of hard particles, whereas the crater formed in Fig. 7a and Fig. 8a can be thought as due to multiple cracking of hard phase and dislodging of the fragments. Other than that silica particles are embedded in the coated sample (Fig. 7c, Fig. 8b and Fig. 9d). In all images, we notice that the penetration of silica in to the sample is very small. This is a distinct feature compared to penetration of silica in to plain Ti-31 (Fig. 9d).Similar interactions between erodent and hard composite coating is reported elsewhere [24-26].

When hard erodent impacts soft matrix phase present in the composite coating, the matrix phase undergoes plastic deformation. If sharp edge of the angular erodent faces the sample surface, it generates ploughing and groove action. Both generate flow lips. Ploughing introduces more plastic deformation and strain hardening. Compared Ti-31 alone, the matrix phase in the composite coating is less ductile and the local material (where erodent impacts) becomes brittle. This region is prone to cracking and spalling due to extensive strain hardening.

Table III Comparison of angle of impingement and steady state volume erosion rate

Angle of Impingement	Uncoated Material($cm^3/gX10^{-5}$)	Coated Material($cm^3/gX10^{-5}$)
30^0	0.8	4
60^0	0.75	5.5
90^0	0.4	7

From Table III, Fig.2 and Fig.6, It shows the comparison of uncoated and coated samples of erosion rate versus angle of impingement. It confirmed that erosion rate is very low initially and increases gradually(Fig.2) and in coated samples erosion rate is high initially and gradually becomes constant erosion rate(Fig.6).In coated samples, erodent particles are stuck on top surface of substrate and avoids the further erosion rate as compared with the uncoated samples. In uncoated samples, erosion rate is not constant and continuously degrade the material.

V. CONCLUSION

Higher erosion loss observed for 10% Al_2O_3-CoCrAlTaY coating is attributed to brittle mode of erosion and higher porosity in the coating. The embedment of silica particles into the open porosity are evident from the micrograph which resulted in deeper craters, erosion behavior (brittle) of the coating resulting from extensive plastic flow.

Substrate alloys exhibit lower steady state volume erosion rate in comparison to HVOF coating under test conditions. The higher hardness ratio between silica erodent particle and substrate alloys might have caused the penetration of silica particles in to the surface which bestow some shielding effect against impacting particles leading to lower wear loss. Also, the uncoated alloys being ductile in nature plastic deformation and strain hardening contributes for increased erosion resistance.

REFERENCES

1. Mahesh Anuwar, Jayganthan, R., Tewari, V.K., Arivazhagan, N. Materials Letters, 61, (2007) 1483-1488.
2. Ramesh M.R, Satya Prakash, Nath, S.K., PawanKumar Sapra, Venkataraman, B. Wear, 269, (2010) 197-205.
3. Sundararajan, G. Wear, 186-187, (1995) 129-144.
4. Finnie, I., Proceedings of the Third U.S. National Congress of Applied Mechanics, (1958) 527-532
5. Finnie, I., Wear, 3, (1960) 87-103.
6. Finnie, I. Wear, 186-187, (1995) 1-10.
7. Matthews, A., Areley, Holiday, P. Mater. World, 6, (1998) 346-347.
8. Stringer John. Materials Science and Engg., 87, (1987) 1-10.
9. Gurrappa, I. Materials Science and Tech., 19, (2003) 178-183.
10. Rodríguez, J., Martín, A., Fernández, R., Fernández. Wear, 255, (2003) 950-955.
11. Subhash Kamal, Jayaganthan, R., Satya Prakash, Sanjay Kumar. Journal of Alloys and Compounds, 463, (2008) 358-372.
12. Murthy, K.N., Rao, D.S., Venkataraman, B., Wear, 249, (2001) 592-600.
13. Hutchings, I.M. Edward Arnold Publication, 225, (1992) 825-834.
14. Sidhu, T.S., Malik, A., Prakash, S., Agarwal, R.D, Journal of Thermal Spray Technology, 16(5-6), (2007) 844-849.
15. Kumar, S., Subramany Sarma, Murthy, B.S. Materials Science and Engineering, 476, (2008) 333-340.
16. Mishra, S.B., Prakash.S., Chandra, K, Wear, 260, (2006) 422-432.
17. Al-Fadhli, H.Y., Stokes, J., Hashmi, M.S.J., Yilbas, B.S, Surface and Coatings Technology, 200, (2006) 5782-5788.
18. Hazoor Singh Sidhu, Buta Singh Sidhu and Prakash, S., Surface and Coatings Technology, 202, (2007) 232-238.
19. Sundararajan, G. Wear, 145, (1991) 251-282.
20. Sheldon, G.L., Finnie, I., Journal of Eng. Ind. Trans. ASME, 88, (1966) 393-400.
21. Lawn, B. and Wilshaw., Journal Mater. Sci., 10, (1975) 1049-1081.
22. Soderberg, S., Hogmark, S., Engman, U., Swahn, H. Tribology International, 14(6), (1981) 333-343.
23. Soderberg, S., Hogmark, S., Engman, U., Swahn, H. Tribology International, 14(6), (1981) 333-343.
24. Zambelli, Levy, Wear, 68(3), (1991) 305-331.
25. Wensink, Elwenspoek, Wear, 253, (2002) 1035-1043.
26. Hussainova, I., Kubarsepp, J., Shcheglov, I. Tribology, Int., 32, (1999) 337-344.

AUTHORS PROFILE

Anand Babu K, is working as a Assistant Professor in REVA University,Bengaluru. He has published 4 Journal papers, Current area of research are Surface Engineering, Composite Materials.

Dr. Jegadeeswaran, N is working as a Professor in REVA University, Bengaluru. He obtained his doctoral degree in the area of Thermal coatings on turbine alloys from NITK, Surathkal. He has published 9 peer reviewed journals papers and more than 15 international conferences. Presently he is guiding 6 PhD scholars. Current area of research are corrosion, oxidation and erosion and thermal coatings.

Dr. Kapilan N, is working as a HOD and Professor in Nagarjuna college of Engineering and Technology, Bengaluru. He has published 25 reputed journals and received grants from DST and VGST. He is a Core working committee member ISHRAE Bengaluru chapter. Current area of research is Bio-fuels and HVAC.

Dr. Ramesh M R, is working has a Associate Professor in National Institute of Technology Karnataka, Surathkal. He has published 73 reputed journals and two book chapters. Current area of research is Thermal Spray Coatings, Thin films, Laser and microwave surface modification, Biomaterials, Machining, Wear, Erosion, Oxidation & Hot Corrosion and Severe Plastic Deformation.